Static and dynamic structure of liquid lithium

1994 J. Phys.: Condens. Matter 6 3849

(http://iopscience.iop.org/0953-8984/6/21/010)

J. Phys.: Condens. Matter 6 (1994) 3849–3864. Printed in the UK

Static and dynamic structure of liquid lithium

D J González†, L E González† and K Hoshino‡

† Departamento de Física Teórica, Facultad de Ciencias, Universidad de Valladolid, 47011 Valladolid, Spain

‡ Faculty of Integrated Arts and Sciences, Hiroshima University, Higashi-Hiroshima 724, Japan

Received 5 January 1994

Abstract. We present theoretical calculations for the temperature dependence of both the static and the dynamic structure of liquid lithium. Our approach is based on the neutral pseudoatom method to obtain the screening valence electron density around a Li^+ ion as well as the effective interatomic pair potential, and on the variational modified hypernetted chain integral equation theory of liquids to obtain the liquid static structure. Then, the dynamic structure is calculated in the viscoelastic approximation. This combination results in a whole theory free of adjustable parameters. The results obtained show rather good agreement with the available simulation and experimental data.

1. Introduction

Among the metallic systems, lithium has the simplest electronic structure, two s core electrons and one valence electron, which is not matched by a similar simplicity in the understanding of its properties. Even among the alkali metals, lithium shows rather peculiar behaviour, such as being virtually immiscible with all other alkali metals, which, in turn, are miscible between themselves (Potter and Rand 1985), and it also poses very specific problems for the experimental determination of its liquid structure (Albas 1983, Rupperberg and Reiter 1982, Ruppersberg *et al* 1980, Visser *et al* 1980, Olbrich *et al* 1983). In fact, some differences appear between the static structure factors of liquid lithium depending on whether they have been obtained by x-ray or neutron diffraction experiments. In x-ray experiments the analysis of the data is less certain than for other metals, because the effects of delocalization of the conduction electrons are rather large. The analysis of the x-ray data requires the atomic form factor (which is the Fourier transform of the electronic density), and although the usual procedure has been to use the electronic density corresponding to the free atom, this may not be correct for metallic lithium, since one out of three electrons is delocalized. Moreover, the inelastic (Compton) scattering is rather substantial for lithium (as compared with the other alkali metals), and the theoretical calculations of the Compton scattering also suffer from inadequate knowledge of the implications of the delocalization effects. On the other hand, for neutron diffraction experiments, the Placzek correction is larger than usual because of the small atomic mass of the lithium nucleus, and it is not yet clear whether the usual corrections are adequate.

On the theoretical side, the understanding of the properties of simple metals, that is (s, p)-bonded metals, has usually been closely linked to the idea of a pseudopotential. Within the alkali group, it is expected that the pseudopotential for Li be quite different in comparison with the other alkali metals. Li has only two s electrons in the core and the p

0953-8984/94/213849+16$19.50

valence electrons feel the full electron–ion potential, whereas for the other alkalis both the s and p components are expected to be weak. Hence the pseudopotential of Li should be stronger and more non-local than the pseudopotential for the other alkalis.

Although a first-principles pseudopotential is a very complicated non-local and energy-dependent operator, it has been shown (Hafner and Heine 1983) that a qualitative understanding of the main structural trends in solid and liquid simple metals can be achieved even by using the simplest local pseudopotential, that is, Ashcroft's empty-core model potential (Ashcroft 1966).

Several local and non-local pseudopotentials have been proposed for lithium (Ashcroft 1966, Dagens *et al* 1975, Hoshino and Young 1986, Li *et al* 1987, Chihara 1989, Das and Joarder 1990, Jank and Hafner 1990, Walker and Taylor 1990). We have recently carried out a study on the characteristics of some of these pseudopotentials by computing their predicted structural and thermodynamic properties for liquid lithium in several thermodynamic states (González *et al* 1993a). In that study we have also proposed a new local pseudopotential that incorporates some important electronic properties, namely, the screening valence electronic density, as computed from first principles. Recently, the dynamic structure of liquid lithium has been studied by inelastic neutron scattering experiments (de Jong *et al* 1992, 1993, Verkerk *et al* 1992, de Jong 1993) and by molecular dynamics simulations (Canales *et al* 1993).

The purpose of this paper is to extend the previous work (González *et al* 1993a) to study theoretically the static structure, that is, ion–ion and electron–ion correlations, as well as the dynamic structure of liquid lithium at several temperatures. This is carried out by using a recently developed very accurate integral equation of liquids, the variational modified hypernetted chain (VMHNC) equation (Rosenfeld 1986), and an effective interionic pairwise additive interaction obtained from the neutral pseudoatom (NPA) method (Dagens 1972, 1973, 1975, González *et al* 1993b). Therefrom, the dynamical structure is obtained on the basis of the viscoelastic approximation. The ensuing combination results in a body of theory free of adjustable parameters. The theoretical results are discussed in comparison with the results of the experiment as well as the simulation.

2. Theory

2.1. Effective interionic potentials: the neutral pseudoatom model

A liquid metal can be regarded as a conduction electron gas of mean number density n_e moving through an assembly of ions, with charge Z_v and mean ionic density $\rho = n_e/Z_v$, whose configuration is random in space and time. Moreover, the ions attract the valence electrons, which pile up around them, thus screening the ionic potential and leading to an effective interaction between the ions.

In this section we briefly describe the method for obtaining the interatomic pair potentials. For further details we refer the reader to the literature (Perrot 1990, Perrot and March 1990, González *et al* 1993b).

The computation of the effective interatomic potential incorporates two distinct steps: first, the valence electron density displaced by an ion embedded in a homogeneous electron gas is calculated by using the NPA model; and secondly, we construct an effective local pseudopotential, which, within linear response theory (LPT), reproduces the same displaced density as obtained in the first step. Finally, the effective interatomic potential is obtained from the pseudopotential.

Within the NPA model, it is assumed that the total electron density, $\rho_e(r)$, of the metal can be decomposed as a sum of localized electronic densities, $n(r)$, that follow the ions in their movement,

$$\rho_e(r) = \sum_i n(|r - R_i|) = \sum_i n_c(|r - R_i|) + \sum_i n_v(|r - R_i|) \tag{2.1}$$

where R_i denotes the ionic positions, $n_c(r)$ is the core electronic density and $n_v(r)$ is the valence electronic density, whose computation is the main aim of the NPA. This is carried out by decomposing the valence electronic density, $n_v(r)$, into two contributions $n'_v(r)$ and $n''_v(r)$, namely $n_v(r) = n'_v(r) + n''_v(r)$. The first contribution arises when an ion is introduced into a jellium in which a cavity has been made, so $n'_v(r)$ represents the valence electronic density displaced by the external potential

$$V'_{ion}(r) = V_{ion}(r) + [(1/r) * \nu(r)] \tag{2.2}$$

where $*$ denotes the convolution operation, $V_{ion}(r)$ stands for the ionic potential and $\nu(r)$ is a cavity screening function introduced in order to make $V'_{ion}(r)$ as weak as possible. The total charge of $\nu(r)$ is equal to Z_v, the valence of the ions, so it will compensate the behaviour of $V_{ion}(r)$ for large distances. On the other hand, for small distances $V_{ion}(r)$ diverges as $-Z_{at}/r$, where Z_{at} is the atomic number of the ions, so $V'_{ion}(r)$ will not be weak. Moreover, the contribution of the core electrons to $V'_{ion}(r)$ is influenced by the presence of the valence electrons, so $V'_{ion}(r)$ and $n'_v(r)$ must be evaluated self-consistently. This has been done through the density-functional theory (DFT), by solving the Kohn–Sham equations for all the electrons (core and valence electrons), where the electronic exchange and correlation effects have been taken into account in the local-density approximation (LDA) by using the expression of Vosko *et al* (1980).

The second contribution to the valence electronic density, namely $n''_v(r)$, represents the electronic density that screens in LRT the charge distribution given by the cavity screening function $\nu(r)$, that is

$$\tilde{n}''_v(q) = -(4\pi/q^2)\chi(q)\tilde{\nu}(q) \tag{2.3}$$

where the tilde denotes the Fourier transform and $\chi(q)$ is the density response function, in which the electronic exchange and correlation effects have been included through the LDA local-field correction, so as to be consistent with the approximations made in the previous step. For more details about the use of the LRT and the optimum shape of the cavity, we refer the reader to Dagens (1972), Perrot (1990) and González *et al* (1993b), and we only mention that for the present calculations we have used a spherical cavity with radius given by the Wigner–Seitz radius R_{WS}.

Now, we turn to the calculation of a local pseudopotential, $\tilde{v}_{ps}(q)$, which within LRT reproduces the non-linear screening charge determined by the NPA method, namely $n_v(r)$. This is achieved by first pseudizing $n_v(r)$ so as to eliminate the core orthogonality oscillations, leading to a displaced valence electronic pseudo-density, $n_{ps}(r)$, from which a pseudopotential is obtained by

$$\tilde{n}_{ps}(q) = \chi(q)\tilde{v}_{ps}(q). \tag{2.4}$$

Finally, standard second-order pseudopotential perturbation theory leads to an effective interatomic pair potential, $\phi(r)$, given by

$$\phi(r) = Z_v^2/r + \phi_{ind}(r) \tag{2.5}$$

where the Fourier transform of $\phi_{ind}(r)$ is given by

$$\tilde{\phi}_{ind}(q) = \chi(q)|\tilde{v}_{ps}(q)|^2. \tag{2.6}$$

This completes the specification of the NPA method as we have applied it to compute the interatomic pair potentials of liquid lithium in different thermodynamic states.

2.2. Liquid static theory: the variational modified hypernetted chain approximation

The calculation of the static structural functions of the liquid system has been carried out by using the variational modified hypernetted chain (VMHNC) approximation, which is briefly described below. For further details see Rosenfeld (1986) and González *et al* (1992).

The starting point of most integral equation theories of liquids is the Ornstein–Zernike equation, which for a homogeneous, isotropic system can be written as

$$h(r) = c(r) + \rho \int c(|\mathbf{r} - \mathbf{r}'|)h(\mathbf{r}')\,\mathrm{d}\mathbf{r}' \tag{2.7}$$

which defines the direct correlation function, $c(r)$, in terms of the total correlation function, $h(r) = g(r) - 1$, where $g(r)$ is the pair distribution function. This relation is supplemented by the exact closure relation

$$c(r) = h(r) - \ln\{g(r)\exp[\beta\phi(r) + B(r)]\} \tag{2.8}$$

where $\phi(r)$ is the interatomic pair potential, $\beta = (k_B T)^{-1}$ is the inverse temperature and $B(r)$ denotes the bridge function, for which some approximation must be made. Following the universality assumption of the bridge function (Rosenfeld and Ashcroft 1979), we have chosen that obtained within the Percus–Yevick (PY) approximation for the hard-spheres (HS) system with a packing fraction η, that is, $B(r) = B_{\mathrm{PY}}(r, \eta)$. This function depends only on the single parameter η and the procedure to determine it has led to different—though closely interwoven—approaches. The VMHNC criterion to determine this parameter, as a function of the thermodynamic state, is to minimize a virial/energy thermodynamically consistent local Helmholtz free-energy functional $f^{\mathrm{VMHNC}}(\beta, \rho, \eta)$ with respect to variations in η. The variational condition

$$\partial f^{\mathrm{VMHNC}}(\beta, \rho, \eta)/\partial\eta = 0 \tag{2.9}$$

determines $\eta = \eta(\beta, \rho)$. In the above equation

$$f^{\mathrm{VMHNC}}(\beta, \rho, \eta) = f^{\mathrm{MHNC}}(\beta, \rho, \eta) - \Delta_\phi(\eta) \tag{2.10}$$

where $f^{\mathrm{MHNC}}(\beta, \rho, \eta)$ stands for the MHNC free-energy functional (Rosenfeld 1986) and $\Delta_\phi(\eta)$ is given by

$$\Delta_\phi(\eta) = \tfrac{1}{2}\rho \int_0^\eta \mathrm{d}\eta' \int \mathrm{d}r\, g_{\mathrm{PY}}(r, \eta')\frac{\partial B_{\mathrm{PY}}(r, \eta')}{\partial\eta'} - \delta_\phi(\eta). \tag{2.11}$$

Here the term $\delta_\phi(\eta)$ is a fitting function, which for reasons discussed elsewhere (Rosenfeld 1986, González *et al* 1992) is chosen as

$$\delta_\phi(\eta) = f_{\mathrm{CS}}(\eta) - f_{\mathrm{PYV}}(\eta) \tag{2.12}$$

where $f_{\mathrm{PYV}}(\eta)$ and $f_{\mathrm{CS}}(\eta)$ denote the Percus–Yevick virial and the Carnahan–Starling free energies for the hard-sphere system (Young 1987), respectively. The procedure to obtain the structure of the system is to minimize $f^{\mathrm{VMHNC}}(\beta, \rho, \eta)$ with respect to variations in η; the optimized value of η is used to evaluate the HS–PY bridge functions, substitute these in equation (2.8) and solve this equation coupled with equation (2.7) to find the static ion–ion correlation functions.

2.3. Electron–ion correlation functions

The correlation between valence electrons and ions can be described by the electron–ion structure factor $S_{ei}(q)$ and its Fourier transform, the electron–ion pair distribution function $g_{ei}(r)$, which, within the linear response approximation, are simply obtained as (Chihara 1987)

$$S_{ei}(q) = Z_v^{-1/2}\tilde{n}_v(q)S(q) \tag{2.13}$$

and

$$g_{ei}(r) = 1 + \frac{1}{(n_e\rho)^{1/2}}\frac{1}{(2\pi)^3}\int S_{ei}(q)\exp(i\boldsymbol{q}\cdot\boldsymbol{r})\,d\boldsymbol{q}. \tag{2.14}$$

Here $\tilde{n}_v(q)$ stands for the Fourier transform of the screening valence electronic density, $n_v(r)$, and $S(q)$ represents the ion–ion static structure factor.

3. Results

The present formalism has been applied to study the static and dynamic structural characteristics of liquid lithium at three different temperatures for which experimental neutron scattering results are available (Olbrich *et al* 1983). Table 1 summarizes the thermodynamic states, namely temperatures and ionic number densities, for which the present calculations have been carried out.

Table 1. Thermodynamic states studied in this work.

T (K)	470	595	725
ρ (Å^{-3})	0.0445	0.043	0.042

3.1. Screening valence electron density and effective interatomic potentials

The first step in our study concerns the calculation of the electronic 1s core states of a Li^+ ion as well as its self-consistent screening valence electronic density $n_v(r)$, which are computed as pointed out in section 2.1. As is shown in figure 1, the screening valence electronic density shows an oscillatory behaviour; the small oscillation in the core region is due to $n'_v(r)$ and it is related to the orthogonality condition between the valence and the core electronic wavefunctions, whereas the greater oscillation in the core region is due to $n''_v(r)$. The oscillations of $n_v(r)$ at large values of r are the well known Friedel oscillations, and their behaviour is also mainly determined by $n'_v(r)$. This can be appreciated in the inset of figure 1, which shows, for $T = 470$ K, the screening valence electronic density $n_v(r)$ along with its two components, $n'_v(r)$ and $n''_v(r)$. Also, in figure 1 we have plotted the screening valence electronic densities for two temperatures and, for comparison, we have also included the 2s-electron density distribution of a free Li atom, $n_{2s}(r)$. It is observed that an increase of temperature leads to a further spreading out of the screening valence electronic densities. Also, it is worth noting that the liquid metal screening valence electronic densities are similar to the atomic 2s-electron density distribution, although the atomic one is less spread out and does not show oscillations for large r values. On the other hand, the computed

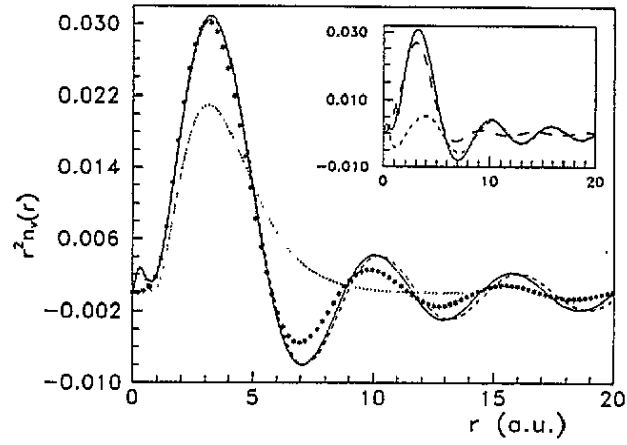

Figure 1. Total screening valence electronic density, $r^2n_v(r)$, for Li at $T = 470$ K (full curve) and $T = 725$ K (broken curve). The dotted curve represents the 2s-electron density in a free Li atom and the asterisks show the total screening valence electronic density obtained for Li at $T = 470$ K by using the Ashcroft model potential. The inset shows, for $T = 470$ K, a comparison between $r^2n_v(r)$ (full curve) and its two components, $r^2n'_v(r)$ (short broken curve) and $r^2n''_v(r)$ (long broken curve).

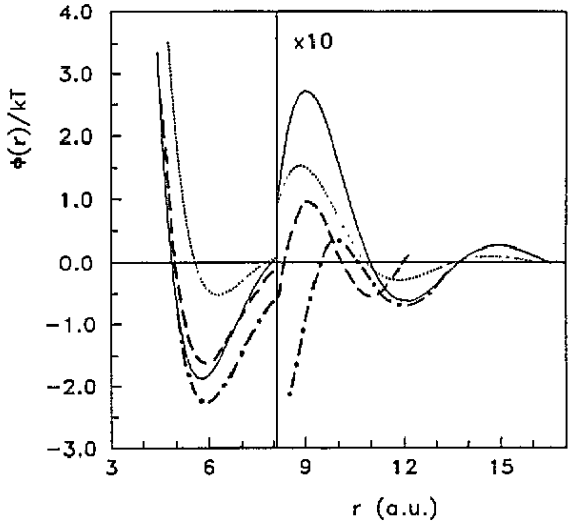

Figure 2. Interatomic pair potentials for Li at $T = 470$ K: full curve, NPA result; broken curve, OPW result of Jank and Hafner (1990); chain curve, QHNC result of Chihara (1989); dotted curve, result obtained by using Ashcroft's empty-core model potential (González *et al* 1993a).

electronic density distribution corresponding to the 1s core electrons is practically the same as that of the 1s electrons in the free atom.

Now, from the previously obtained screening valence electronic densities, the effective interatomic pair potentials are easily derived according to the prescription outlined in section 2.1. It should be mentioned that by applying equation (2.4) we are generating an effective local pseudopotential; this has been made in order to avoid the introduction of

adjustable parameters while at the same time preserving the full information contained in our calculated screening valence electronic density. In this way a pseudopotential in the linear response regime is built up so as to generate a non-linear screening charge determined by the NPA method.

Several local and non-local pseudopotentials have already been proposed for lithium (Ashcroft 1966, Dagens *et al* 1975, Hoshino and Young 1986, Li *et al* 1987, Chihara 1989, Das and Joarder 1990, Jank and Hafner 1990, Walker and Taylor 1990) and in a previous work (González *et al* 1993a) we have studied some of them by comparing their predicted structural and thermodynamic properties; now in the present work we will concentrate on three of them that have a parameter-free character. First, we should mention the non-local Heine–Abarenkov type pseudopotential of Dagens *et al* (1975), which was obtained by a very similar NPA type calculation, although these authors did not take into account the electronic correlation and their $V_{\text{ion}}(r)$ (see equation (2.2)) was taken from the free ion instead of the self-consistent one obtained in the present calculation. Another non-local pseudopotential, based on an orthogonalized plane-wave (OPW) expansion of the conduction band states and the LDA for the electronic exchange and correlation, has been proposed by Jank and Hafner (1990). Also, Chihara (1989) has obtained an effective local pseudopotential for lithium, on the basis of the DFT in the quantal hypernetted chain approximation (QHNC), where the liquid metal is modelled as a mixture of nuclei and electrons.

The interatomic pair potentials derived from those different pseudopotentials are shown, for $T = 470$ K, in figure 2. They are rather similar in the repulsive part, the main differences being located in the region of the first attractive minimum where the QHNC-derived pair potential shows a wider and deeper first attractive minimum. The present NPA-derived pair potential stands between both QHNC- and OPW-derived pair potentials and also shows stronger Friedel oscillations.

Nevertheless, besides those differences, the three interatomic pair potentials share the common property of leading to a rather strong interaction with rather similar values for the position of the first attractive minimum. This can be better appreciated by comparing them with the pair potential obtained by using Ashcroft's simple empty-core pseudopotential (Ashcroft 1966) with a core radius, r_c, fitted to match the first peak position of the experimental static structure factor ($r_c = 1.44$ au).

3.2. Static correlation functions

From the previously computed effective interatomic pair potentials, the corresponding various static correlation functions have been obtained according to the formalism outlined in sections 2.2 and 2.3. First, the static ion–ion structure factor, $S(q)$, of liquid lithium at three different temperatures has been computed by using the VMHNC theory, which we have already shown to be a very reliable theory of liquids (González *et al* 1991, 1992), and the results are shown in figure 3. Comparison with the experimental neutron scattering results of Olbrich *et al* (1983) shows, for the three thermodynamic states considered in this work, an overall excellent agreement for both the phase and amplitude of the oscillations; the only exception is the first peak height, where our theoretical results predict a 5% lower value. This is rather remarkable as our theoretical calculations do not resort to any adjustable parameter. The comparison is shown in figure 3 where, for the sake of clarity, we have only plotted the experimental results at $T = 470$ K.

Good agreement has also been obtained by Chihara (1989) within the QHNC-derived interatomic pair potential, although his theoretical result predicts a smaller amplitude for the second peak of $S(q)$. In his calculation, the bridge function was approximated by

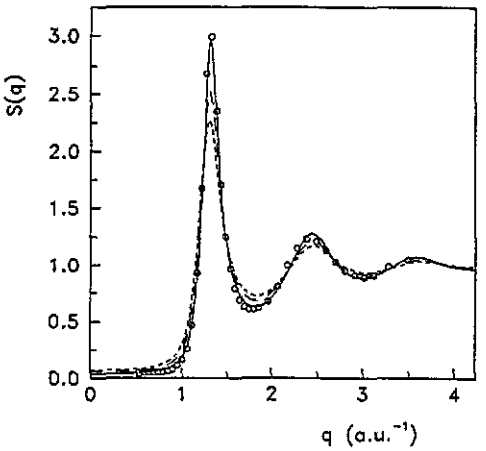

Figure 3. Static structure factor $S(q)$ for Li at T = 470 K (full curve), T = 595 K (long broken curve) and T = 725 K (short broken curve) as obtained from the NPA pair potentials. The open circles are the neutron diffraction data of Olbrich *et al* (1983) for T = 470 K.

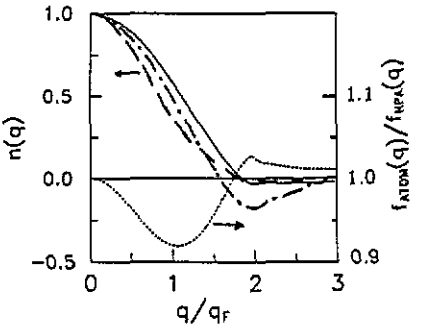

Figure 4. X-ray scattering form factor of liquid lithium at T = 470 K. The full curve is the result from the NPA screening valence electron density, the broken curve is from the atomic 2s electron density and the chain curve is the theoretical result of Visser *et al* (1980). In the figure (RHS scale) we have also represented the ratio between the total (including the core electrons) NPA form factor ($f_{NPA}(q)$) and the atomic one ($f_{ATOM}(q)$).

the PY–HS bridge function, $B_{PY}(r, \eta)$, with the parameter η chosen so as to match the experimental value of $S(q = 0)$. Also, good agreement was obtained by Jank and Hafner (1990) by performing a molecular dynamics simulation with their OPW-derived interatomic pair potentials, although the oscillations of their theoretical $S(q)$ are slightly out of phase in comparison with the experimental one.

For liquid lithium at T = 470 K, there are also experimental x-ray scattering results, $S_X(q)$, by Waseda (1980), that show some important discrepancies with the neutron scattering results, $S_N(q)$, of Olbrich *et al* (1983): (i) within the range 1.2 Å^{-1} $\leqslant q \leqslant$ 2.0 Å^{-1} there are some appreciable differences, with $S_N(q)$ being smaller than $S_X(q)$; (ii) the main peak of $S_N(q)$ is higher by about 10%; and (iii) for bigger q values there appears a systematic shift in the oscillations. In fact, some of these discrepancies may be explained in terms of the form factor used to reduce the raw data obtained from an x-ray scattering experiment, where the usual procedure is to resort to the atomic form factor. Figure 4 shows the ratio between the form factor obtained from the present NPA calculations, $f_{NPA}(q)$, and that found by using the atomic electron density, $f_{ATOM}(q)$. It is found that, up to $q \simeq 2.1$ Å^{-1}, $f_{NPA}(q) > f_{ATOM}(q)$, and therefore the use of $f_{NPA}(q)$ would reduce the value of $S_X(q)$ so as to bring it closer to $S_N(q)$. On the other hand, in the region around the main peak position of $S(q)$, $q \simeq 2.5$ Å^{-1}, $f_{NPA}(q) < f_{ATOM}(q)$, which now would enhance $S_X(q)$ and reduce the discrepancy with $S_N(q)$.

Now, by applying equations (2.13) and (2.14), the electron–ion correlation functions are easily obtained. First, in figure 4 we have plotted the Fourier transform of the screening valence electron density, $\tilde{n}_v(q)$, which appears in equation (2.13) as obtained for T = 470 K, and in figure 5 we show the electron–ion structure factors, $S_{ei}(q)$, associated with the three thermodynamic states considered in this work. From this figure several interesting features of $S_{ei}(q)$ must be mentioned: (i) they are positive in the long-wavelength region where the temperature dependence is more strongly reflected; (ii) they show a dip at the

position of the main peak of the ion–ion structure factor, and its magnitude decreases with increasing temperature; and (iii) after the first dip, $S_{ei}(a)$ quickly becomes positive again and decays smoothly to zero. All these features are in qualitative agreement with the experimental results obtained by Takeda *et al* (1986, 1989) for other metallic systems, and our theoretical results for $S_{ei}(q)$ also show that its temperature dependence is mainly driven by the temperature dependence of the ion–ion structure factor.

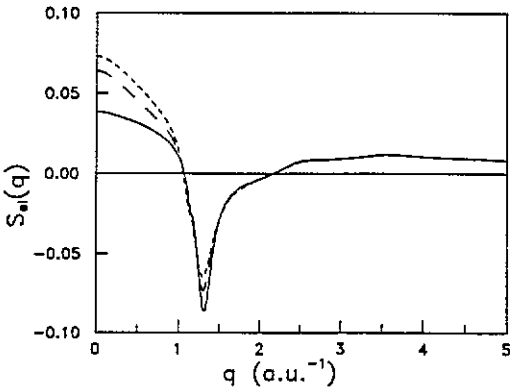

Figure 5. Electron–ion static structure factors $S_{ei}(q)$ for Li at $T = 470$ K (full curve), $T = 595$ K (long broken curve) and $T = 725$ K (short broken curve).

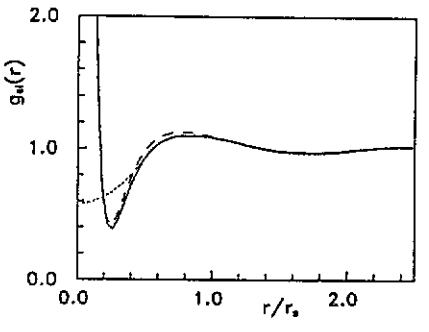

Figure 6. Electron–ion pair distribution functions $g_{ei}(r)$ for Li at $T = 470$ K (full curve) and $T = 725$ K (broken curve) as obtained from the total screening valence electron density. The dotted curve shows, for $T = 470$ K, the $g_{ei}(r)$ obtained by using the pseudo-density, $n_{ps}(r)$.

Figure 6 shows the calculated electron–ion pair distribution functions, $g_{ei}(r)$, for two temperatures, and the following characteristic features can be appreciated: (i) there is a dip at a distance of about 0.85 au, which appears as a consequence of the orthogonality condition between the valence and the 1s core wavefunctions; (ii) its oscillatory behaviour is rather weak, with a broad first maximum followed by broad and strongly damped oscillations; and (iii) its temperature dependence is also rather weak, as compared with the behaviour of the ion–ion pair distribution function. In this figure we have also included the $g_{ei}(r)$ obtained by using in equation (2.13) the screening electronic valence pseudo-density, $\tilde{n}_{ps}(q)$. It shows that, by sweeping away the core orthogonality oscillations of the screening valence electronic density, as is done in a typical pseudopotential calculation, the structure of the $g_{ei}(r)$ inside the core region is also swept away and, just outside the core region, a realistic description of the $g_{ei}(r)$ can be obtained.

3.3. Dynamic structure

From the previously obtained interatomic pair potential $\phi(r)$ and the pair distribution function $g(r)$, we can obtain the frequency $\omega_L(q)$ defined as

$$\omega_L^2(q) = 3\omega_0^2(q) + (\rho/m)\int g(r)[1-\cos(qz)]\frac{\partial^2\phi(r)}{\partial z^2}\,d\boldsymbol{r} \tag{3.1}$$

where

$$\omega_0^2(q) = q^2(k_B T/m) \tag{3.2}$$

and m stands for the ionic mass. In fact, these frequencies are related to the second and fourth frequency moments of the dynamic structure factor, $S(q,\omega)$, as

$$\int_{-\infty}^{\infty}\omega^2 S(q,\omega)\,\mathrm{d}\omega=\omega_0^2(q)\qquad\int_{-\infty}^{\infty}\omega^4 S(q,\omega)\,\mathrm{d}\omega=\omega_0^2(q)\omega_L^2(q). \tag{3.3}$$

Now, the dynamic structure factor has been calculated within the framework of a simple viscoelastic model in which the second-order memory function of the intermediate scattering function is assumed to decay exponentially with a relaxation time $\tau(q)$. This assumption leads to an $S(q,\omega)$ given by (Hansen and McDonald 1986)

$$S(q,\omega)=\frac{1}{\pi}\frac{\tau(q)\omega_0^2(q)[\omega_L^2(q)-\omega_0^2(q)/S(q)]}{\{\omega\tau(q)[\omega^2-\omega_L^2(q)]\}^2+[\omega^2-\omega_0^2(q)/S(q)]^2} \tag{3.4}$$

and for the decay rate $1/\tau(q)$ we have taken the simple expression (Lovesey 1971)

$$\tau^{-1}(q)=(2/\sqrt{\pi})[\omega_L^2(q)-\omega_0^2(q)/S(q)]^{1/2} \tag{3.5}$$

which leads to the correct ideal-gas value of $S(q,\omega)$ for large q and small ω values. In fact, this approximate scheme has also been successfully applied to study the temperature dependence of the dynamical structure of liquid rubidium (Hoshino *et al* 1992).

The dynamics of liquid lithium has been studied experimentally by inelastic neutron scattering (de Jong *et al* 1992, 1993, Verkerk *et al* 1992, de Jong 1993) and by inelastic x-ray scattering (Burkel 1991). In fact, de Jong *et al* measured the total dynamic structure factor of liquid lithium at $T=470$, 526 and 574 K; the data obtained suggest the existence of collective modes (sound modes) from about $0.64q_p$ (where q_p denotes the main peak position of $S(q)$, $q_p\simeq 2.5$ Å^{-1}), since the experimental set-up did not allow the observation of collective modes for smaller q-values. On the other hand, the experimental results obtained by Burkel (1991) at $T=600$ K also point to the existence of collective modes within the ranges $0.12q_p\leqslant q\leqslant 0.8q_p$ and $1.2q_p\leqslant q\leqslant 1.45q_p$.

In figure 7 we show the theoretical $S(q,\omega)$ obtained for several q-values, along with the corresponding molecular dynamics (MD) results obtained by Canales *et al* (1993) using also the present NPA-derived interatomic pair potential. It is observed that the calculated $S(q,\omega)$ show well defined peaks for small q-values ($q\leqslant 1.8$ Å^{-1}), whereas for larger q-values there are no maxima and the values of $S(q,\omega)$ increase up to $q=2.5$ Å^{-1}, which corresponds to the main peak position of the static structure factor, q_p. As shown in figure 7, these trends are in complete agreement with the MD results (Canales *et al* 1993). In fact, except for q-values smaller than q_p, a fair agreement is obtained between the present theoretical and the corresponding MD results. This is rather remarkable considering the simplicity of the approximation employed here. A better description of $S(q,\omega)$ would require more elaborate approximations, such as the self-consistent scheme, to obtain the memory function (Bosse *et al* 1978, Sjögren 1980).

We note that in the MD simulations of Canales *et al* (1993) a window function was used so as to remove the cut-off noise in the Fourier transform of the intermediate scattering function, $F(q,t)$. It is well known that this procedure introduces some broadening and lowering of the peaks and, in order to quantify this effect and also to make a more meaningful comparison with the MD results, we have also studied the changes induced in our theoretical results by applying the same window function to the theoretical $F(q,t)$. The new obtained results for $S(q,\omega)$ show, in general, rather small differences with the previous ones, which

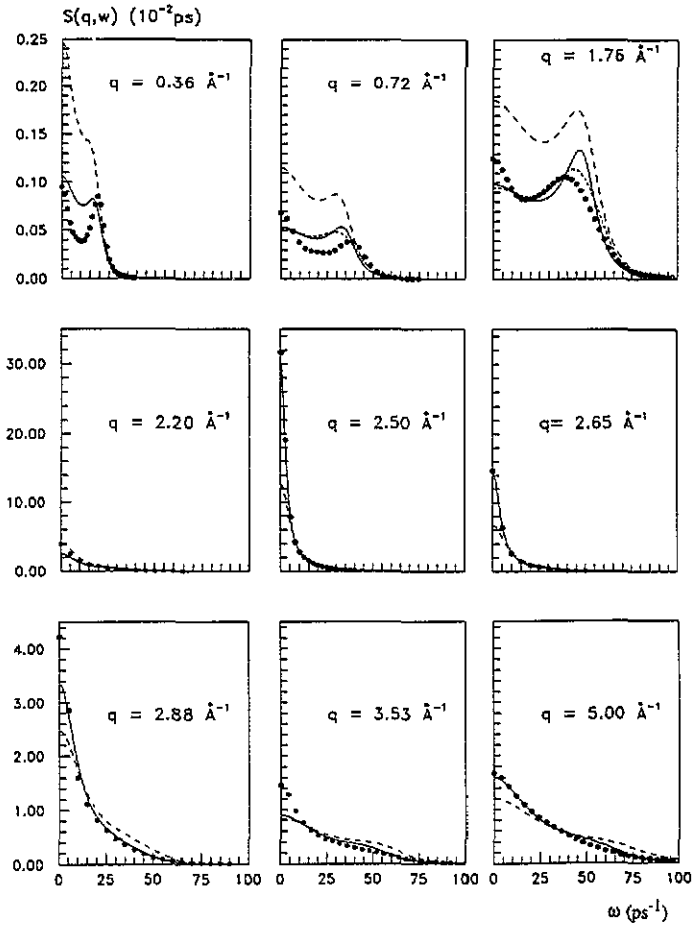

Figure 7. Dynamic structure factors $S(q, \omega)$ for different q-values. The full and broken curves show the present theoretical results for $T = 470$ and 725 K, respectively, and the full circles are the molecular dynamics results of Canales *et al* (1993). The dotted curve, for $q = 0.72$ and 1.76 Å^{-1}, denotes the $S(q, \omega)$ obtained by applying the same window function as used in the MD simulations (Canales *et al* 1993).

are hardly noticeable within the scale of figure 7. Nevertheless, for $q = 0.72$ and 1.76 Å^{-1} a small but appreciable lowering of the peak occurs, and for these cases we have also included in figure 7 the new dynamic structure factor.

Now, the longitudinal current density correlation function, $C_l(q, \omega) = \omega^2 S(q, \omega)$, is easily obtained. This function shows for all q-values and $\omega > 0$ a clear maximum, and the frequencies of the maxima for the different q-curves lead to the (longitudinal) dispersion relation ($\omega_l^m(q)$). Within the viscoelastic approximation, $\omega_0(q)/\sqrt{[S(q)]}$ and $\omega_L(q)$ give the lower and upper bounds of the dispersion relation, i.e. $\omega_0(q)/\sqrt{[S(q)]} < \omega_l^m(q) < \omega_L(q)$, and in figure 8 we have plotted these frequencies for liquid Li at $T = 470$ and 725 K along with the corresponding MD results (Canales *et al* 1993). The agreement of the theoretical $\omega_l^m(q)$ with the MD result at $T = 470$ K is reasonably good.

By comparing the result for $T = 470$ K with that for $T = 725$ K we can observe the characteristic features of the temperature dependence of the dispersion curve. That is, as the temperature increases: (i) the dispersion curve does not appreciably change for q-values

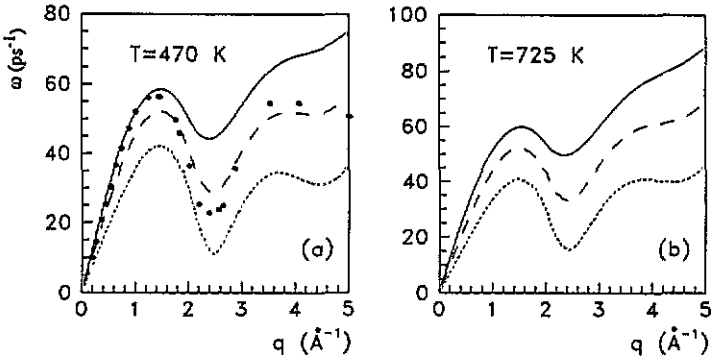

Figure 8. Calculated dispersion curves $\omega_l^m(q)$ (broken curve), $\omega_L(q)$ (full curve) and $\omega_0(q)/\sqrt{[S(q)]}$ (dotted curve) for (*a*) = 470 K and (*b*) T = 725 K. The full circles represent the $\omega_l^m(q)$ values obtained from MD simulation (Canales *et al* 1993).

in the range $q < 1.5$ Å^{-1} (which is the position of the first peak of $\omega_l^m(q)$); (ii) the first minimum at $q \simeq 2.5$ Å^{-1} (which corresponds to the position of the first peak of $S(q)$) becomes shallower, and this is mainly due to the temperature dependence of $S(q)$ (see figure 3); and (iii) $\omega_l^m(q)$ increases with temperature for $q > 2.5$ Å^{-1}. These characteristic features of the temperature dependence of $\omega_l^m(q)$ have also been obtained theoretically for expanded liquid rubidium (Hoshino *et al* 1992) and are consistent with both the experimental (Pilgrim *et al* 1991) and the MD simulation (Kahl *et al* 1993) results for liquid rubidium.

As previously stated, the present theoretical $S(q,\omega)$ do show maxima only for q-values smaller than 1.8 Å^{-1}. These maxima, denoted by $\omega_B(q)$, show for small q a rather linear behaviour, leading to a theoretical value of the adiabatic velocity of sound of $c_s \simeq 4700$ m s^{-1}. This value is slightly higher than the corresponding experimental value of 4550 m s^{-1}. A similar agreement has recently been obtained for liquid Na at $T = 380$ K by MD simulations (Shimojo *et al* 1993).

The viscoelastic expression for the dynamic structure factor $S(q,\omega)$ can, alternatively, be written as

$$S(q,\omega) = [S(q)/\pi]\,\mathrm{Re}\,\tilde{F}(q, z = \mathrm{i}\omega) \tag{3.6}$$

where $\tilde{F}(q, z = \mathrm{i}\omega)$ is a sum of three complex Lorentzian functions

$$\tilde{F}(q, z = \mathrm{i}\omega) = \frac{A_-(q)}{z + z_-(q)} + \frac{A_0(q)}{z + z_0(q)} + \frac{A_+(q)}{z + z_+(q)} \tag{3.7}$$

with $A_0(q)$ and $z_0(q)$ being real functions whereas $A_\pm(q)$ and $z_\pm(q)$ are either real or complex conjugate. The parameters $z_0(q)$ and $z_\pm(q)$ satisfy the following equations (Lovesey 1984)

$$\begin{aligned} &z_0 + z_+ + z_- = 1/\tau \\ &z_0 z_+ + z_0 z_- + z_+ z_- = \omega_L^2 \\ &z_0 z_+ z_- = [\omega_0^2/S(q)](1/\tau) \end{aligned} \tag{3.8}$$

where we have dropped the argument q and τ has already been defined in equation (3.4). This set of equations is easily reduced to a third-degree polynomial whose (real and

complex) solutions are readily obtained. The parameter $z_0(q)$ represents the halfwidth at half maximum (HWHM) of the Rayleigh peak of $S(q,\omega)$, whereas $\mathrm{Re}[z_\pm(q)]$ represent the HWHM of the Brillouin peaks of $S(q,\omega)$ that are centred at $\omega = \mathrm{Im}[z_\pm(q)]$. This alternative form of $S(q,\omega)$ enables a closer comparison with the recent analysis of experimental inelastic neutron scattering data (de Jong *et al* 1993, de Jong 1993). In that study, the total dynamic structure factor was decomposed into its self and collective parts by using models for $S_s(q,\omega)$ and $S(q,\omega)$ respectively. The Nelkin–Ghatak model (Lefevre *et al* 1972) was used for $S_s(q,\omega)$, whereas for $S(q,\omega)$ a sum of three Lorentzian functions (equation (3.7)) was employed. The whole fitting procedure involved several free parameters and the results obtained (which we have included in figures 9 and 10) show rather large error bars, which are due to the different results obtained by using different initial guesses for those fitting parameters. Nevertheless, as pointed out by de Jong (1993), the analysis of the obtained data for $T = 526$ and 574 K suggests the existence of collective modes around q_p and beyond; on the other hand, the corresponding data for $T = 470$ K are rather inconclusive as for the appearance of a sound propagation gap around q_p.

By using our theoretical results for $\omega_L(q)$ and $S(q)$ we have solved equations (3.8) and the results obtained are shown in figures 9 and 10. First, in figure 9 we show a comparison between the theoretical and experimental results for $z_0(q)$, $\mathrm{Re}[z_\pm(q)]$ and $\mathrm{Im}[z_\pm(q)]$ corresponding to $T = 470$ K, whereas in figure 10 a similar comparison is carried out although now the theoretical results are for $T = 595$ K and the experimental ones are for $T = 575$ K. Note that figures 9(*c*) and 10(*c*) represent the dispersion relation of the collective modes. Although the experimental error bars are rather large, the wavenumber dependence of these magnitudes is qualitatively well described by the simple viscoelastic theory.

4. Summary

In this paper we have investigated the static and dynamic structure of liquid lithium in three different thermodynamic states. The present theoretical approach, which is parameter-free, is based on an effective interatomic pair potential derived from the neutral pseudoatom approach, on the variational modified hypernetted chain approximation to obtain the static structure and on the viscoelastic theory to obtain the dynamic structure. For the static structure, the good agreement found between theoretical and experimental results gives further coincidence in the present NPA-derived interatomic pair potential. In fact, in a previous work (González *et al* 1993a) we have also shown that this pair potential leads to rather good results for the thermodynamic properties of liquid lithium at several temperatures. For the dynamic structural properties considered in this work, the comparison between the theoretical and the MD results shows that the viscoelastic theory gives a good qualitative account of the characteristic features of the dynamic structure factor and, consequently, of the longitudinal dispersion relation for the sound modes. Furthermore, comparison with the available inelastic neutron scattering data, i.e. the HWHM of the Rayleigh peak and both the position and the HWHM of the Brillouin peaks, shows that, in spite of the large error bars associated with these experimental results, at least their wavenumber dependence can be qualitatively explained by the present theoretical description.

Finally we point out that the present results for the dynamic structure of liquid lithium share some common features with those of other liquid alkali metals; i.e. the temperature dependence of the dispersion curve of liquid lithium is similar to that obtained both experimentally and theoretically for expanded liquid rubidium. On the other hand, Balucani

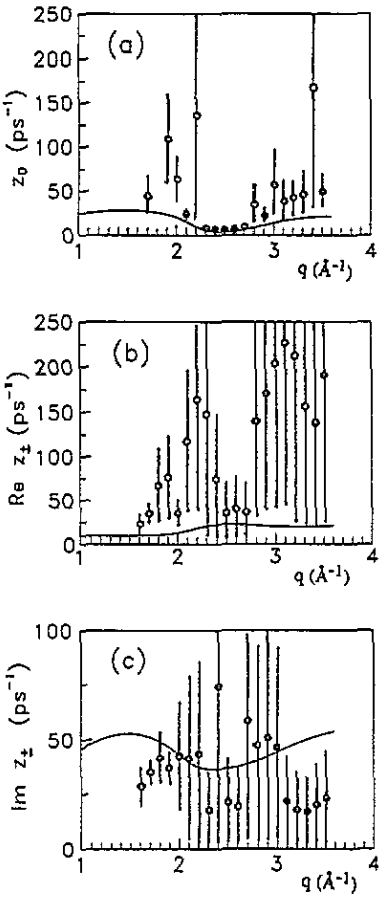

Figure 9. Theoretical (full curve) and experimental (de Jong 1993) (open circles with error bars) results for liquid lithium at $T = 470$ K: (*a*) HWHM of the Rayleigh peak of $S(q, \omega)$; (*b*) HWHM of the Brillouin peak of $S(q, \omega)$; and (*c*) position of the Brillouin peak of $S(q, \omega)$.

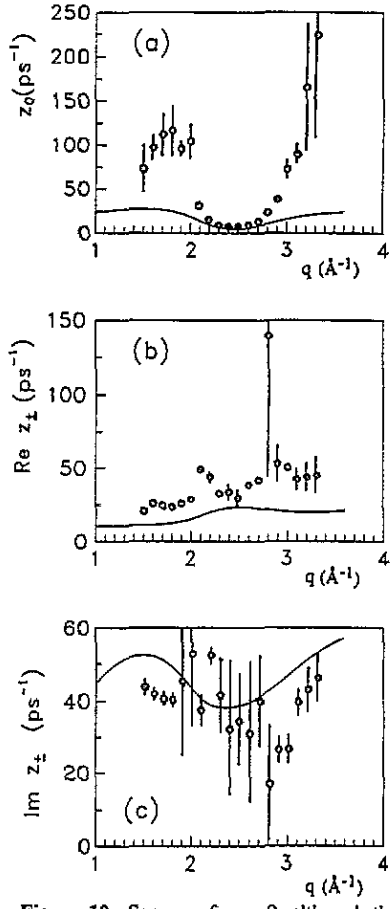

Figure 10. Same as figure 9, although the theoretical results are for $T = 595$ K whereas the experimental ones (de Jong 1993) are for $T = 575$ K.

et al (1992) have shown that the liquid alkali metals (Na, K, Rb and Cs) at their melting point exhibit a 'universal' scaling behaviour for several dynamic and transport properties, so it will be interesting to investigate whether liquid lithium can also be included into that behaviour.

Although the present results for the dynamic structure are rather encouraging, we think that further dynamic properties (i.e. velocity autocorrelation function, diffusion coefficient, shear viscosity, etc) should also be studied in order to ascertain fully the capability of the present theoretical approach. Computations are in progress and will be reported upon completion.

Acknowledgments

DJG gratefully acknowledges the Japanese–German Center, Berlin, for the provision of a

fellowship that made it possible for him to visit Hiroshima University. He also warmly acknowledges the hospitality at the laboratory of Professors M Watabe and K Hoshino where part of this work has been carried out. LEG and DJG also thank the ECC Science Program under Contract Number ERBSC1*CT910754 and the DGICYT of Spain through Grant PB92-0645. We also thank P H K de Jong and P Verkerk for very helpful discussions and for providing us with experimental data prior to publication.

References

Alblas B P 1983 *PhD Dissertation* University of Groningen (unpublished)
Ashcroft N W 1966 *Phys. Lett.* **23** 48
Balucani U, Torcini A and Vallauri R 1992 *Phys. Rev.* A **46** 2159
Bosse J, Götze W and Lücke M 1978 *Phys. Rev.* A **18** 1176
Burkel E 1991 *Inelastic Scattering of X-Rays With Very High Energy Resolution* (Berlin: Springer)
Canales M, Padró J A, González L E and Giró A 1993 *J. Phys.: Condens. Matter* **5** 3095
Chihara J 1987 *J. Phys. F: Met. Phys.* **17** 295
—— 1989 *Phys. Rev.* A **40** 4507
Dagens L 1972 *J. Phys. C: Solid State Phys.* **5** 2333
—— 1973 *J. Physique* **34** 879
—— 1975 *J. Physique* **36** 521
Dagens L, Rasolt M and Taylor R 1975 *Phys. Rev. B* **11** 2726
Das T and Joarder R N 1990 *J. Non-Cryst. Solids* **117/118** 583
de Jong P H K 1993 *PhD Dissertation* University of Delft (unpublished)
de Jong P H K, Verkerk P, Ahda S and de Graaf L A 1992 *Recent Developments in the Physics of Fluids* ed W S Howells and A K Soper (Bristol: Hilger)
de Jong P H K, Verkerk P and de Graaf L A 1993 *J. Non-Cryst. Solids* **156/158** 48
González L E, González D J and Silbert M 1991 *Physica* B **168** 39
—— 1992 *Phys. Rev.* A **45** 3803
González L E, González D J, Silbert M and Alonso J A 1993a *J. Phys.: Condens. Matter* **5** 4283
González L E, Meyer A, Iñiguez M P, González D J and Silbert M 1993b *Phys. Rev.* E **47** 4120
Hafner J and Heine V 1983 *J. Phys. F: Met. Phys.* **13** 2479
Hansen J P and McDonald I R 1986 *Theory of Simple Liquids* 2nd edn (New York: Academic)
Hoshino K and Young W H 1986 *J. Phys. F: Met. Phys.* **16** 1659
Hoshino K, Ugawa H and Watabe M 1992 *J. Phys. Soc. Japan* **61** 2182
Jank W and Hafner J 1990 *J. Phys.: Condens. Matter* **2** 5065
Kahl G, Kambayashi S and Nowotny G 1993 *J. Non-Cryst. Solids* **156/158** 15
Lefevre Y, Chen S H and Yip S 1972 *Neutron Inelastic Scattering* (Vienna: IAEA) p 445
Li D H, Moore R A and Wang S 1987 *J. Phys. F: Met. Phys.* **17** 2007
Lovesey S W 1971 *J. Phys. C: Solid State Phys.* **4** 3057
—— 1984 *Phys. Rev. Lett.* **53** 401
Olbrich H, Ruppersberg H and Steeb S 1983 *Z. Naturf.* **38A** 1328
Perrot F 1990 *Phys. Rev.* A **42** 4871
Perrot F and March N 1990 *Phys. Rev.* A **41** 4521
Pilgrim C, Winter R, Hensel F, Morkel C and Glasser W 1991 *Ber. Bunsenges. Phys. Chem.* **95** 1133
Potter P E and Rand M H 1985 *Handbook of Thermodynamic and Transport Properties of Alkali Metals* ed R W Ohse (Oxford: Blackwell Scientific) ch 9.1
Rosenfeld Y 1986 *J. Stat. Phys.* **42** 437
Rosenfeld Y and Ashcroft N W 1979 *Phys. Rev.* A **29** 1208
Rupperberg H and Reiter R 1982 *J. Phys. F: Met. Phys.* **12** 1311
Ruppersberg H, Saar J, Speicher W and Heitjans P 1980 *J. Physique Coll.* **41** (C8)595
Shimojo F, Hoshino K and Watabe M 1994 *J. Phys. Soc. Japan* **63** 141
Sjögren L 1980 *Phys. Rev.* A **22** 2883
Takeda S, Harada S, Tamaki S and Waseda Y 1986 *J. Phys. Soc. Japan* **55** 3437
—— 1989 *J. Phys. Soc. Japan* **58** 3999
Verkerk P, de Jong P H K, Arai M, Bennington S M, Howells W S and Taylor A D 1992 *Physica* B **180/181** 834
Visser E G, Geertsma W, van der Lugt W and de Hosson J Th M 1980 *Z. Naturf.* **35A** 373

Vosko S H, Wilk L and Nusair M 1980 *Can. J. Phys.* **58** 1200
Walker A B and Taylor R 1990 *J. Phys.: Condens. Matter* **2** 9481
Waseda Y 1980 *The Structure of Non-Crystalline Materials* (New York: McGraw-Hill)
Young W H 1987 *Can. J. Phys.* **65** 241
Ziman J M 1967 *Proc. R. Soc.* **91** 701